Knowledge-based systems using neural networks for electron beam welding process of reactive material (Zircaloy-4)

**M. N. Jha · D. K. Pratihar · A. V. Bapat · V. Dey ·
Maajid Ali · A. C. Bagchi**

Abstract Bead-on-plate welding of zircaloy-4 (a reactive
material) plates was conducted using electron beam accord-
ing to central composite design of experiments. Its predic-
tive models were developed in the form of knowledge-based
systems in both forward and reverse directions using neural
networks. Input parameters considered for this welding of
reactive metals were accelerating voltage, beam current and
weld speed. The responses of the welding process were
measured in terms of bead width, depth of penetration and
micro-hardness. Forward mapping of the welding process
was conducted using regression analysis, back-propagation
neural network (BPNN), genetic algorithm-tuned neural net-
work (GANN) and particle swarm optimization algorithm-
tuned neural network (PSONN). Reverse mapping of this
process was also carried out using the BPNN, GANN and
PSONN-based approaches. Neural network-based approaches
could model this welding process of reactive material in both
forward and reverse directions efficiently, which is required
for the automation of the same. The performance of the neural
network models was found to be data-dependent. The BPNN
could outperform the other two approaches for most of the
cases but not all in both the forward and reverse mappings.

Keywords Electron beam welding · Knowledge-based
system · BPNN · GANN · PSONN

M. N. Jha · A. V. Bapat · M. Ali · A. C. Bagchi
Bhabha Atomic Research Centre, Trombay, Mumbai 400085, India

D. K. Pratihar (✉) · V. Dey
Department of Mechanical Engineering, Indian Institute
of Technology, Kharagpur 721302, India
e-mail: dkpra@mech.iitkgp.ernet.in

Introduction

Zircaloy-4 (Zr-4), a reactive material, is used as a fuel
cladding in Pressurized Water Reactors (PWR) and CANa-
dian Deuterium Uranium (CANDU) reactors due to its excel-
lent corrosion resistance, good mechanical properties and
very low thermal neutron cross-section. Zirconium alloys
have low linear coefficient of thermal expansion giving supe-
rior dimensional stability at the elevated temperatures mak-
ing it most suitable for nuclear waste containers, where the
temperature could exceed 200 °C for hundreds of years.[1]
Zr-4 is also used for the fabrication of reprocessing plant
equipment due to its outstanding general corrosion resistance
in nitric acid media and insensitivity to intergranular corro-
sion (Tonpe et al. 2011). It is a reactive metal and has a strong
affinity for oxygen and nitrogen at elevated temperatures and
is considered to be in the difficult-to-weld category. Zr-4
material can be welded by Tungsten Inert Gas (TIG) welding
and Electron Beam Welding (EBW) process. The hardness
value in the TIG welded region is found to be higher than that
in the base metal region reducing its ductility. The increase
in hardness may be due to the increase in oxygen or nitrogen
content in the weld region (Thomas et al. 1993). Zr-4 can be
welded using EBW process in vacuum without the danger of
becoming brittle due to contamination.

EBW is an autogenous welding process, in which intense
heat energy required to melt and fuse the metal is obtained
by the impingement of highly focused beam of electrons
on to the target surface. It has the potential to become the
most important technology for the welding of light weight
alloy and reactive metals for nuclear industry, aerospace and

national defense applications (Thomas et al. 1993; Chi and Chao 2007).

The mechanical properties of the welded joint, such as yield strength, tensile strength, and micro-hardness are determined as a part of the weld qualification, which depend on the metallurgical properties and physical dimensions of the weld bead and heat affected zone (Lancaster 1970). These metallurgical and physical properties depend on the input process parameters, namely accelerating voltage, beam current, welding speed, focus positions, ambient pressure, and others. The input-output correlations are required to be developed in both forward and reverse directions to predict the outputs of the process for a given set of input parameters and vice-versa, that is, to determine the required set of process parameters in order to obtain the desired outputs in real time. This is required for the automation of the process. The problem of forward modeling can be solved using statistical regression analysis. However, it may not be always possible to carry out the reverse modeling using the obtained regression equations. As regression analysis is conducted response-wise, it may not be able to capture the complete information of the process. On the other hand, modeling involving multiple inputs and outputs can be done simultaneously using neural networks. The training of a knowledge-based system is provided off-line and after the training is over, it can be used on-line. Thus, knowledge-based systems (also known as expert systems) could be useful to establish the said relationships of a process in both the directions.

Literature review

A considerable amount of work had been carried out by various investigators to study the welding of reactive materials. Some of those studies are discussed here. Saresh et al. (2007) studied the effects of EBW on thick Ti-6Al-4V titanium alloy and found that contamination must be avoided to obtain the sound weld. The authors concluded that cosmetic pass might be required to eliminate the undercuts, which was very detrimental. Rao et al. (2008) studied the fracture toughness of EB welded Ti-6Al-4V, and found that these values of the weld metals were superior to that of the base metal. Choi and Choi (2008) investigated the effects of welding conditions on the mechanical properties of pure titanium and found that the specimen with minimum number of welding pass and maximum amount of shielding gas could give rise to the highest tensile strength. Saha and Ray (2008) presented the requirements of vacuum level and welding speed for welding of various reactive metals. Zircaloy used for nuclear applications should be welded at an ambient pressure of less than 2×10^{-4} mbar. Tonpe et al. (2011) studied the corrosion resistance property of EB welded and TIG welded Zr-4 plates and found that its corrosion resistance values in boiling 11.5M

nitric acid was better than that of any other potential material used for reprocessing equipment fabrication. However, it was also found that the hardness of the weld region of TIG welded samples were more than double the hardness value in the base metal region. On the other hand, the hardness value increased by only 7.6 % for the EB welded plates. Ahmad et al. (2002) conducted the hardness and microstructural studies of electron beam welded joints of Zr-4 and stainless steel plates. They found that the defects like porosity, voids and cracks could be avoided and heat affected region was reduced in EBW.

Though some qualitative studies involving microstructure characterization of reactive metal welding using EBW had been conducted, the study of input-output modeling of EBW process for the reactive metals has not yet been reported. The mathematical models for the EBW process had been developed by various researchers (Hashimoto and Matsuda 1965; Klemens 1969; Miyazaki and Giedt 1982; Vijayan and Rohatgi 1984; Elmer et al. 1990; Petrov et al. 1998; Ho 2005) correlating the input process parameters with the outputs or responses. The analytical models require exact distribution of the heat flux, power density and physical properties of the material at elevated temperatures, which are difficult and time consuming to measure. Moreover, reverse mapping of the EBW process might not be always possible to carry out using analytical models. In such situations, the models are developed based on the outcomes of experiments performed according to some statistical designs and then analyzed by regression methods to predict the required output. Regression analysis was used by various researchers (Yang et al. 1993; Gunaraj and Murugan 1999a, b, 2000a, b; Ganjigatti et al. 2007) for modeling several conventional welding phenomena. Modern welding processes, such as laser beam welding (LBW) and EBW were also modeled using the regression analysis. Benyounis et al. (2005) utilized Response Surface Methodology (RSM) to predict weld profile in laser welding of medium carbon steel. Koleva (2001, 2005) used statistical regression analysis to develop the correlation of input parameters with the weld parameters for electron beam welding of austenitic stainless steel. Dey et al. (2009) used non-linear regression analysis to predict the bead profile in bead-on-plate welding of stainless steel (SS) 304 plates using electron beam.

Several attempts were made to carry out input-output modeling of various welding processes in forward direction using statistical regression analysis. However, the regression analysis is carried out response-wise and consequently, may not be able to capture the complete information of the process. These problems could be solved using neural network-based approaches.

Neural networks (NNs) can be used to develop knowledge-based systems of the processes in the form of some quantitative models (Bhadeshia 1999). NN-based models had been

used extensively for the modeling of various conventional (Nagesh and Datta 2002; Tay and Butler 1997; Kim et al. 2005, 2002; Dutta and Pratihar 2007; Mollah and Pratihar 2008; Amarnath and Pratihar 2009) and modern welding processes. Vitek et al. (1998) used an NN to model pulsed Nd-YAG laser welds of Al-alloy and found it to be a powerful tool for predicting the weld pool shape characteristics. Plasma arc welding process was modeled by Cook et al. (1995) using an artificial neural network (ANN). They also observed that ANNs are efficient tools for the analysis, modeling and control of this process. Olabi et al. (2006) optimized the welding parameters in terms of ratios of penetration to fuse-zone-width and penetration to HAZ-width for CO_2 laser welding of medium carbon steel using a back-propagation neural network (BPNN). They reported the strength of ANNs in investigating and calculating the optimal penetration depth and widths of fusion zone and HAZ. Okuyucu et al. (2007) developed an ANN model for correlating the welding parameters and mechanical properties for friction stir welding (FSW) process and found that the ANN calculated mechanical properties were in good agreement with the measured data. Dey et al. (2010a, b) used BPNN, genetic algorithm-tuned neural network (GANN) and radial basis function neural network (RBFNN) for the modeling of bead-on-plate welding process using electron beam. Input-output relationships of the butt welding of SS304 plates were investigated by Jha et al. (2011) in both forward and reverse directions using BPNN and GANN, and the latter was found to perform better than the former. Huang and Kovacevic (2011) applied back-propagation neural network and multiple regression analysis for the input-output modeling of the laser beam welding of high strength steel. The laser power, welding speed and acoustic signatures acquired during the laser welding process were taken as the input parameters, whereas weld depth of penetration was considered as the output of the process. They could predict the weld depth of penetration reasonably well by the proposed models. Lin (2012) used the combination of Taguchi Method, Grey relational analysis and neural network for the modeling and optimization of the quality of Gas Metal Arc (GMA) welding. The quality characteristics of the GMA welding process was represented by a single value of grey relational grade determined by normalizing the depth of penetration, depth-to-width ratio and fusion area for each specimen. A multilayer feed-forward neural network was utilized for modeling the process. The quality of GMA welding could be improved using the NN-predicted optimal parameters.

The problems related to forward mapping had been solved by various researchers, but those related to reverse mapping did not receive much attention, till date. The main objective of the present study is to establish input-output correlations of the electron beam welding of reactive metal Zr-4 in both forward and reverse directions in the form of knowledge-based
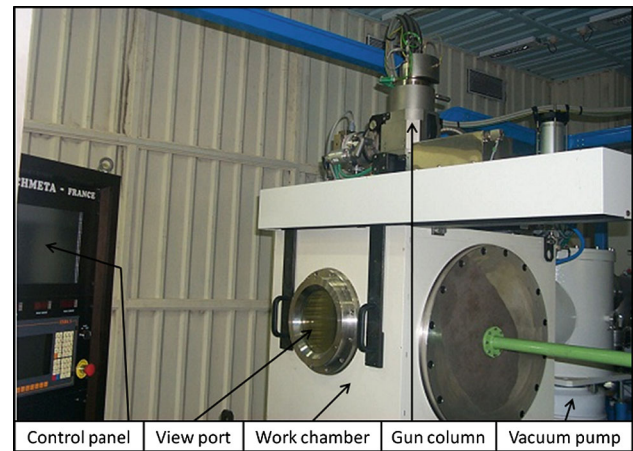

Fig. 1 60 kV, 8 kW Electron beam welding machine

systems, which might be required for its automation. It is important to mention that a knowledge-based system is nothing but an expert system (developed in the form of computer program), which contains the piece of knowledge necessary to establish input-output relationships of a process. [2] Comparisons of the developed knowledge-based systems were made in terms of their performances. Three input process parameters, namely accelerating voltage, beam current and welding speed were considered for the electron beam welding of reactive metals. The responses of the process were measured in terms of weld bead width, depth of the fusion zone and micro-hardness.

The remaining part of this paper is organized as follows: the next section deals with the descriptions of experimental details and data collection methods adopted in the present study. The method of analysis is explained after that. Results are then stated and discussed. Some concluding remarks are made and the scopes for future work are stated at the end.

Experiments and data collection

Bead-on-plate welding experiments on the reactive material: Zr-4 were carried out using 60 kV, 8 kW Techmeta, France make EBW machine located at Atomic Fuels Division, Bhabha Atomic Research Centre, Trombay, Mumbai, India. Figure 1 displays the EBW machine used for the experiments, which consists of electron beam gun column, work chamber, job handling system, job viewing system, power supply, control panel and vacuum pumping system. The work chamber of the EBW machine having the dimensions of $600\,\text{mm} \times 600\,\text{mm} \times 600\,\text{mm}$ was evacuated to a base vacuum in the range of 5×10^{-5} mbar to 3×10^{-5} mbar during the experiments using a diffusion pump assembly backed

---

[2] Available from http://www.cs.ru.nl/~peterl/eolss.pdf.

Table 1 Process parameters and their ranges for electron beam welding of Zr-4 plates

Inputs	Unit	Coded symbol	Un-coded symbol	Minimum value	Mid-value	Maximum value
Accelerating voltage	kV	X_1	V	40	50	60
Beam current	mA	X_2	I	12	16	20
Weld speed	mm/min	X_3	S	600	750	900

by roots-rotary combination of vacuum pumps. The electron beam gun uses indirectly heated tungsten filament as emitter. The gun chamber vacuum of the order of 5×10^{-6} mbar was achieved using turbo-molecular pump backed by a double stage, direct drive rotary vane vacuum pump.

Design of experiments

The significant process parameters for electron beam welding of reactive metals are accelerating voltage (V), beam current (I), weld speed (S), and ambient pressure. The ambient pressure was kept fixed in the range of 5×10^{-5} mbar to 3×10^{-5} mbar during the experiments to avoid any contamination, which may result in the increase of ductile to brittle transition temperature. Three input process parameters, namely V, I, and S were considered within their respective ranges for the electron beam bead-on-plate welding of 4.55 mm thick hot rolled Zr-4 plates (Chemical Composition: Sn = 1.10 %, Fe = 0.23 %, Cr = 0.25 %, O = 1,000 ppm, C = 122 ppm, Zr = 98.41 %). The ranges for V, I and S were decided through a number of trial runs. The experiments were conducted according to central composite design (CCD) methodology (Montgomery 1997), with three center points. Thus, a total of $2^3 + 2 \times 3 + 3 = 17$ combinations of process parameters were considered for the experiments. The process parameters set at their three levels are given in Table 1.

Table 2 shows the CCD matrix considered for the electron beam welding of Zr-4 plates using three factors, each set at its three levels (i.e., two end points and a centre point). Three replicates were considered for each combination of input parameters, and therefore, a total of $3 \times 17 = 51$ experiments were carried out.

Data collection

Experiments were carried out on Zr-4 plates using the combinations of process parameter shown in Table 2. Experiments were also performed for an additional set of eight test cases to be used for verification of the developed models. Table 3 displays the combinations of process parameters used for the test cases.

Bead-on-plate welding was carried out on rectangular Zr-4 plates of dimensions: 90 mm × 30 mm × 4.55 mm. Figure 2 displays some of the EBW bead-on-plate runs on the Zr-4

Table 2 CCD Matrix for electron beam welding of Zr-4 plates

Serial no.	V (kV)	I (mA)	S (mm/min)
1	40	12	600
2	50	16	750
3	60	12	600
4	50	20	750
5	40	12	900
6	40	16	750
7	50	12	750
8	50	16	600
9	40	20	600
10	60	12	900
11	60	20	900
12	50	16	900
13	50	16	750
14	60	20	600
15	40	20	900
16	60	16	750
17	50	16	750

Table 3 Various combinations of process parameters used in the test cases

Serial no.	V (kV)	I (mA)	S (mm/min)
1	45	14	675
2	45	18	675
3	45	14	825
4	45	18	825
5	55	14	675
6	55	18	675
7	55	14	825
8	55	18	825

plates. The Zr-4 plates were cleaned and outgassed before carrying out the bead-on-plate welding.

Cleaning of Zr-4 plates is essential, as contamination may lead to the welds with poor strength and/or poor corrosion resistance (Rudling et al. 2007). The Zr-4 plates were initially cleaned using ethyl alcohol and the cleaned samples were allowed to dry. The cleaned and dried Zr-4 plates were heated in an oven up to 75 °C for about 15–20 min to outgas the moisture adsorbed, if any, due to atmospheric humidity. The
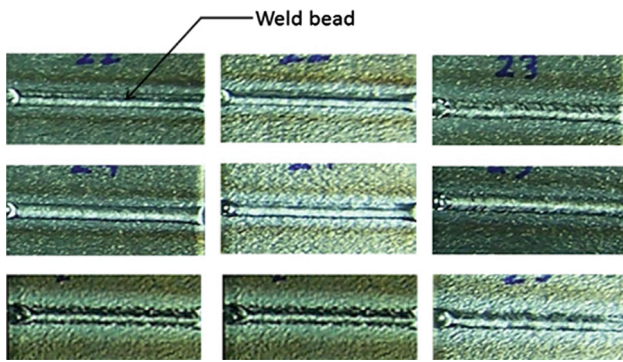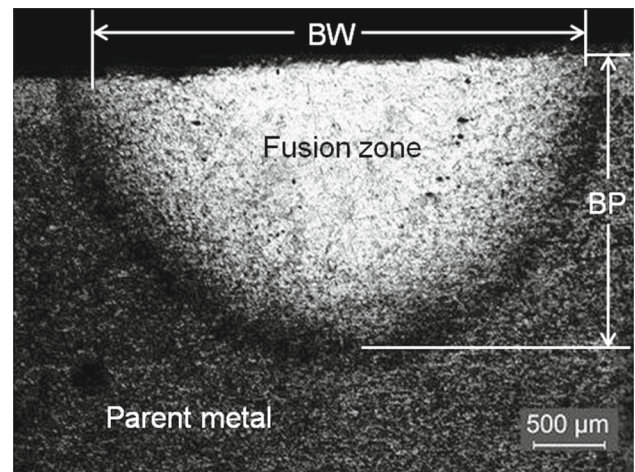
Fig. 2 EBW bead-on-plate runs on Zr-4 plate

Fig. 3 Photograph of the fusion zone profile of 4.55 mm thick Zircaloy-4 plate welded using electron beam

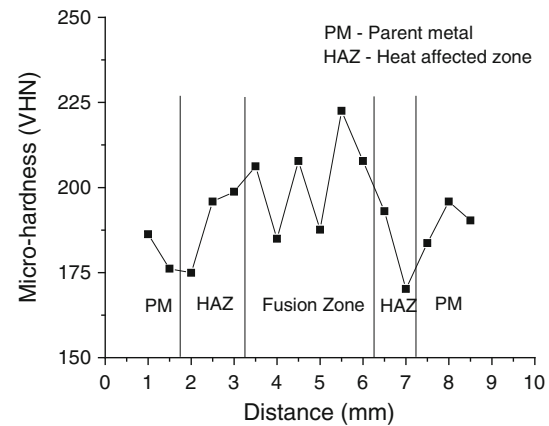Fig. 4 Variations of micro-hardness across the parent metal, HAZ and fusion zone

dried and baked plates were allowed to cool down to room temperature and stored in a humidity-controlled room. The plates were then used for electron beam welding. Welding was carried out with a sufficient inter-pass time, so that the plate comes down to room temperature before the subsequent passes. The EB welded specimens were cut at a minimum distance of 10mm form the edge for preparing cylindrical mounts to be utilized for further analysis. The cylindrical mounts of diameter $\phi 25\,mm \times 25\,mm$ (height) were prepared using cold setting resin. The grinding and polishing of all the mounts were carried out using France make Mecatech 334 polishing machine. The polished samples were etched using chemical solution of $H_2O{:}HNO_3{:}HF$ with a volumetric ratio of 50:45:5.

The output parameters, that is, bead width (BW), bead penetration (BP), and Vickers micro-hardness (Hv) were determined for all the experimental runs and test cases. The bead profiles for all the samples were measured and recorded after taking the images of all the etched samples on Leica make optical microscope. Figure 3 shows the photograph of the fusion zone profile for one of the EB welded samples. The microstructures of fusion zone for some of the EB welded samples of Zr-4 are shown in the "Appendix". The spherical shapes of the fusion zone indicate that a conduction mode of welding was pre-dominant in the EB welding of Zr-4 for the selected ranges of accelerating voltage and beam current.

The micro-hardness values for all the samples were determined along the horizontal direction (across the parent metal, HAZ and fusion zone) at a depth of half of the bead penetration measured from the top. These values were collected using Omni Tech Micro-hardness testing machine using a load of 300 g at room temperature. These values were measured at a separation of $500\,\mu m$ and the average value was used for the modeling and analysis purpose.

Figure 4 displays the variations of micro-hardness measured in a horizontal direction (at a particular depth from the top surface) across the parent metal, HAZ and fusion zone of the weld-bead. The average hardness of the fusion zone was found to be around 9.29 % higher than that of the parent metal and heat affected zone.

Methods of analysis

The models were developed to establish input-output correlations of the electron beam welding of Zr-4 plates using non-linear statistical regression analysis and neural networks as discussed below.

Forward mapping

Electron beam welding process was modeled in the forward direction using non-linear statistical regression analysis and three NN-based algorithms to predict the output(s) or response(s) for a given set of input parameters. Three input parameters, namely accelerating voltage, beam current and welding speed were considered for the model. Three responses, namely weld bead width, bead penetra-

tion and micro-hardness were predicted as the outputs of the model.

Approach 1: Statistical Regression Analysis

A non-linear statistical regression analysis of the data obtained through the experimental runs was carried out using Minitab14 software[3] to establish the input-output relationships. Non-linear regression equation contained a constant, some linear, squared and interaction terms. The values of the constant and coefficients of other terms were determined through a statistical regression analysis by minimizing the error in predictions through the least square technique. Interested readers may refer to Montgomery (1997) for a detailed description of this statistical regression analysis.

Approach 2: Back-Propagation Neural Network

The developed BPNN model consisted of an input layer with three neurons corresponding to the three input parameters, a hidden layer and an output layer with three neurons corresponding to the three outputs. The hidden layer contained 13 neurons, as it was decided through a detailed parametric study. The initial values of connecting weights between the input and hidden layers and those between the hidden and output layers were generated at random. A mean square deviation (MSD) in predictions of the output was minimized in order to obtain the optimal neural network. The MSD in prediction was calculated as follows:

$$MSD = \frac{1}{L}\sum_{l=1}^{L}\frac{1}{M}\sum_{m=1}^{M}\frac{1}{2}\left(T_{om}^{l} - O_{om}^{l}\right)^2, \tag{1}$$

where L denotes the number of training cases, M represents the number of outputs, T_{om}^{l} and O_{om}^{l} indicate the target and predicted outputs, respectively, of mth neuron lying on the output layer corresponding to lth training case. The schematic view of the NN is shown in Fig. 5.

A batch mode of training was adopted to train the network using one thousand training cases. The training cases consisted of 51 scenarios obtained through the real experiments and 949 scenarios generated artificially using the regression equations. The connecting weights: $[V]$ and $[W]$ were updated to reduce the MSD during the training of the network by following the back-propagation algorithm, which works based on the steepest descent method. Interested readers may refer to Pratihar (2008) for a detailed description of the back-propagation algorithm.

Approach 3: Genetic Algorithm-Tuned Neural Network

Figure 6 shows schematic view of a GANN system (Pratihar 2008), in which the back-propagation algorithm of

approach 2 was replaced by a genetic algorithm (GA) in order to evolve an optimal NN system through the batch mode of training. In this model, the NN parameters, such as connecting weights, bias values and transfer functions were optimized using a GA. Each variable of the NN was represented using five bits. The optimum number of hidden neurons was turned out to be equal to 12 through a detailed parametric study. The GA-string looked as follows (for 3 input, 12 hidden and 3 output neurons):

$$\underbrace{10111}_{v_{11}}\ldots\ldots\ldots\ldots\underbrace{10101}_{v_{312}}\underbrace{01110}_{w_{11}}\ldots\ldots\ldots\ldots$$

$$\underbrace{10101}_{w_{123}}\underbrace{10001}_{a_h}\underbrace{01110}_{a_o}\underbrace{10111}_{b}$$

In the above string, v represents connecting weights between input and hidden layers, w denotes connecting weights between the hidden and output layers, a_h and a_o denote the coefficients of log-sigmoid transfer functions for the hidden and output layers, respectively and b represents the bias value. The fitness of the GA-string was calculated using Eq. (1). The GA tried to evolve an optimized NN system through a number of generations using the fitness information calculated on some training scenarios.

Approach 4: Particle Swarm Optimization Algorithm-Tuned Neural Network (PSONN)

In this approach, Particle Swarm Optimization (PSO) algorithm was used to tune the parameters of the NN. The PSO algorithm was proposed by Kennedy and Eberhart (1995) for solving optimization problems. The schematic view of a PSONN system is shown in Fig. 7. The variables, which are required to be optimized, form the population of solutions and are denoted by the particles. Each particle has its own position and velocity to move around the search space. The position of a particle represents a possible solution to the optimization problem and the velocity is directed towards the new and better position. The velocity and position of the ith particle and its dth dimension are changed according to the following equations:

$$v_{id}(t+1) = wv_{id}(t) + c_1 R_1(P_{best} - x_{id}(t))$$
$$+ c_2 R_2(G_{best} - x_{id}(t)), \tag{2}$$

$$x_{id}(t+1) = x_{id}(t) + v_{id}(t+1), \tag{3}$$

where $v_{id}(t)$ represents velocity of the particle at tth iteration, $x_{id}(t)$ indicates its position at tth iteration t, P_{best} is the best previous position of the particle, G_{best} denotes the globally best previous position of the particle, w indicates the inertia weight, c_1 and c_2 represent the cognitive and confidence coefficients, respectively, R_1 and R_2 are the two random numbers lying in the range of (0, 1). The fitness of the PSO particle was calculated using Eq. (1).

---

[3] Available from http://www.minitab.com.
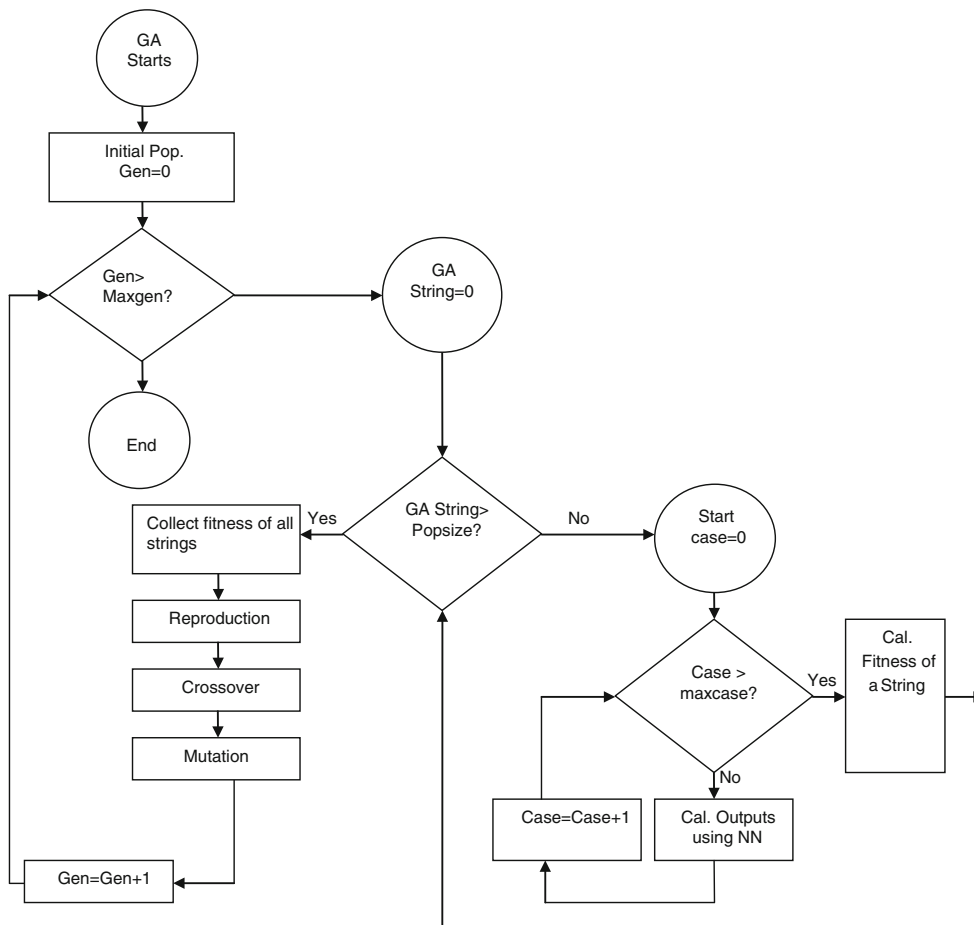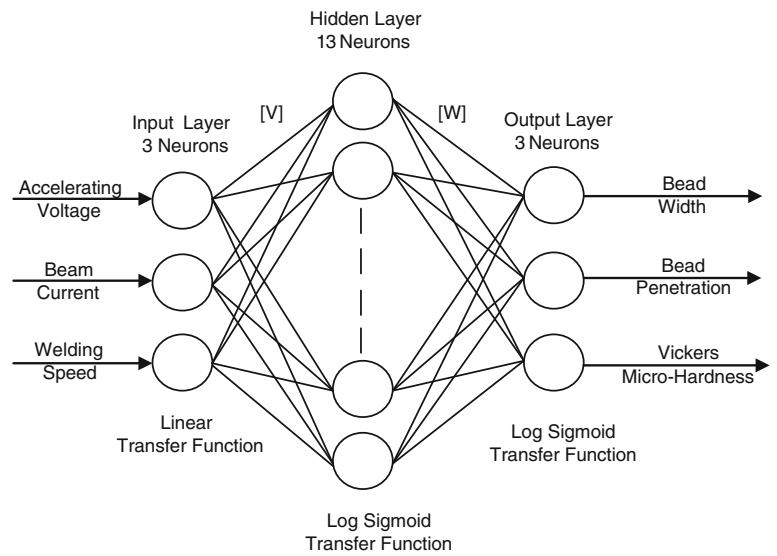
Fig. 5 A schematic view of NN

Fig. 6 A schematic view of GA-NN system (reproduced from the second author's textbook Soft Computing © 2008 Narosa Publishing House, New Delhi Pratihar 2008)
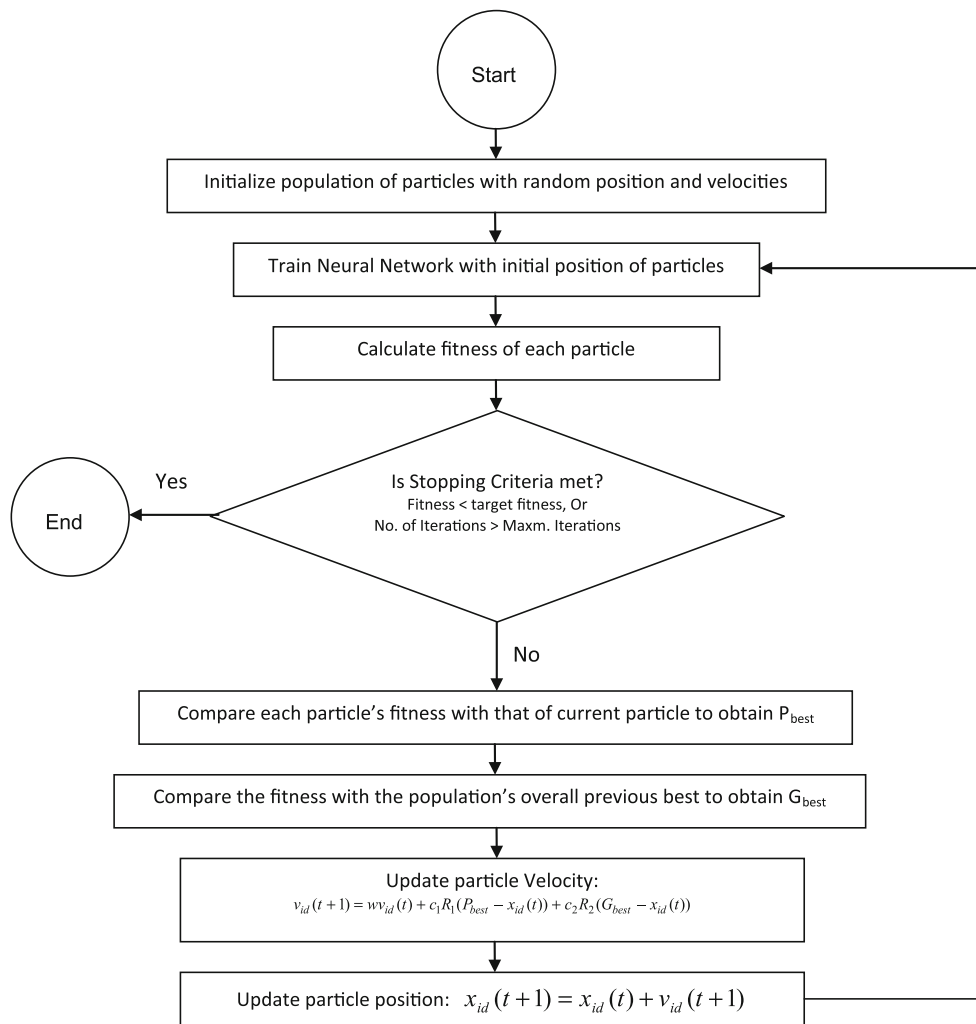
Fig. 7 Flow-chart of PSONN algorithm

It is to be noted that the performance of PSO algorithm depends on its parameters, such as w, c_1, c_2. An optimal NN was evolved by the PSO algorithm through a number of iterations.

Reverse mapping

The reverse mapping of this process was done using BPNN, GANN and PSONN-based approaches. Three desired responses, such as bead width, bead penetration and micro-hardness were fed as inputs to the model and the outputs were obtained in terms of the process parameters to be set to achieve the desired set of responses. The mapping of the process in reverse direction might be required for its automation.

Results and discussion

The input-output models were developed as discussed earlier and the test cases were passed through it to check the adequacy of the model.

Results of forward mapping

Results of Approach 1

The input-output correlations were developed in the forward direction using regression analysis and significance test was conducted to see the effect of process parameters on the responses. The regression analysis was carried out at a confidence level of 95%. The bead-geometric parameters and micro-hardness were represented as the functions of input process parameters as given below.

Weld bead width (BW) Bead Width (BW) was expressed in coded form (refer to Eq. 4) as a non-linear function of process parameters, namely accelerating voltage (V), beam current (I) and welding speed (S), represented by X_1, X_2 and X_3, respectively by using statistical regression analysis, which works based on the principle of the least square error minimization.

$$BW_{coded} = 3.81227 + 0.37183X_1 + 0.61723X_2$$
$$-0.33920X_3 + 0.11886X_1^2 - 0.06781X_2^2$$
$$+0.18536X_3^2 + 0.00892X_1X_2$$
$$+0.02475X_1X_3 - 0.07742X_2X_3 \qquad (4)$$

The terms: X_1, X_2, X_3, and X_3^2 were found to have significant contributions towards BW. Weld bead width was seen to have non-linear relationship with the welding speed (X_3). The bead width was found to vary linearly with accelerating voltage (X_1) and beam current (X_2) considered separately. During the significance test, the coefficient of correlation had turned out to be equal to 0.925 for bead width, which showed that the model was statistically adequate to make further predictions. The adequacy of the model was further confirmed through the analysis of variance (ANOVA). The un-coded form of BW was found to be as follows:

$$BW_{un\text{-}coded} = 6.94930 - 0.0976151V + 0.375553I$$
$$-0.0133790S + 0.00118857V^2$$
$$-0.00423812I^2 + 8.23808E - 06S^2$$
$$+0.000222917VI + 1.65E - 05VS$$
$$-1.29028E - 04IS \qquad (5)$$

Figure 8 displays the surface plots of BW with accelerating voltage, beam current and welding speed. The bead width was seen to increase with increasing beam current and accelerating voltage. Moreover, it decreased with the increasing welding speed. However, the rate of increase in bead width due to the increase in beam current was more than that due to the increase in accelerating voltage. It can be concluded that the welding should be carried out at low beam current and accelerating voltage and high welding speed to obtain small bead width. If the power is required to be increased for obtaining the higher depth of penetration, then it should be increased by increasing the accelerating voltage rather than increasing the beam current to obtain small bead width.

The performance of the developed model was tested on eight test cases. The percent deviations in predictions of bead width are shown in Fig. 9. The maximum value of percent deviation in predictions of BW was found to be equal to 8.67 %. The average absolute percent deviation in predictions of BW had turned out to be equal to 3.07.

Weld bead penetration (BP) The regression analysis was carried out similarly for the BP and the terms: X_1, X_2, X_3, X_2^2,
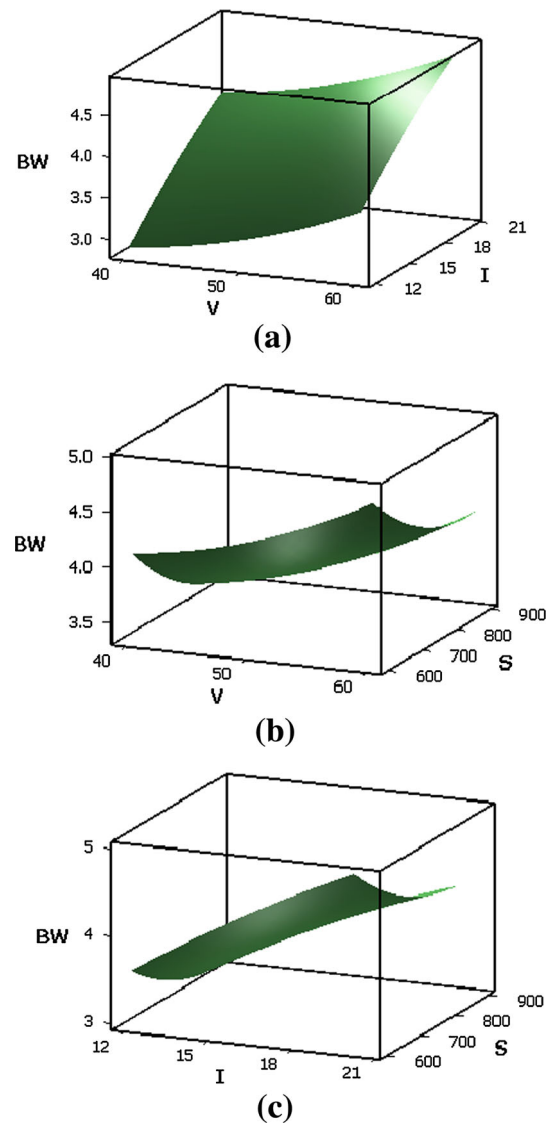

Fig. 8 Surface plots of BW with V, I and S

X_1X_2, and X_2X_3 were found to be significant. The beam current was seen to have non-linear relationship with BP. The BP had shown more or less linear relationship with accelerating voltage and welding speed. The combined effects of X_1X_2 (i.e., VI) and X_2X_3 (i.e., IS) were also found to be significant. The coefficient of correlation was found to be equal to 0.983 for BP. The model was statistically adequate to make further predictions.

The un-coded form of BP was found to be as follows:

$$BP_{un\text{-}coded} = 1.16281 + 0.0268733V - 0.220858I$$
$$-1.57115E - 04S - 5.82958E - 04V^2$$
$$+0.0129190I^2 + 9.07668E - 09S^2$$
$$+0.00368646VI + 2.90833E - 05VS$$
$$-1.95764E - 04IS \qquad (6)$$

Fig. 9 Percent deviation in predictions of BW for the test cases

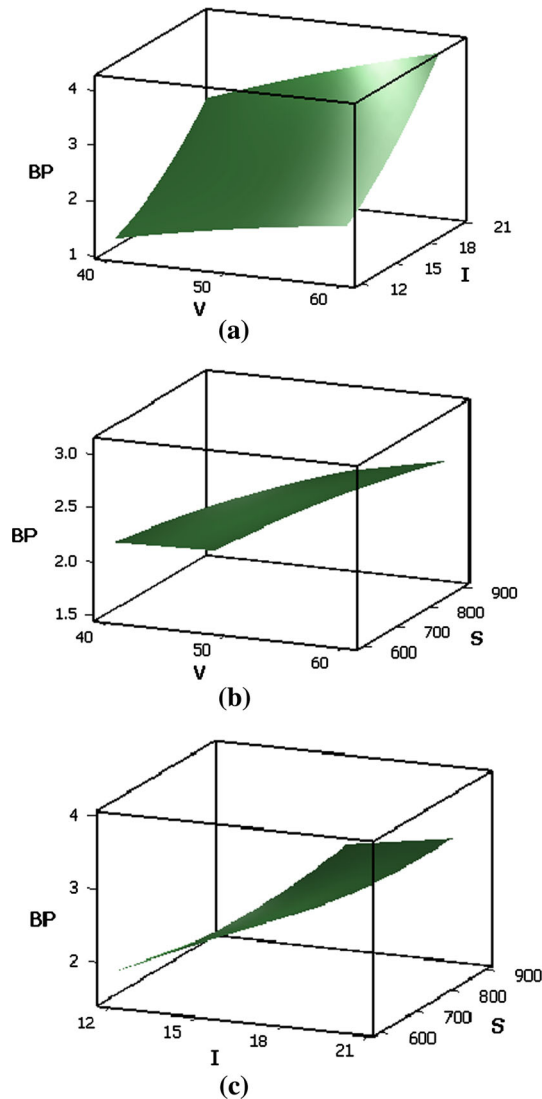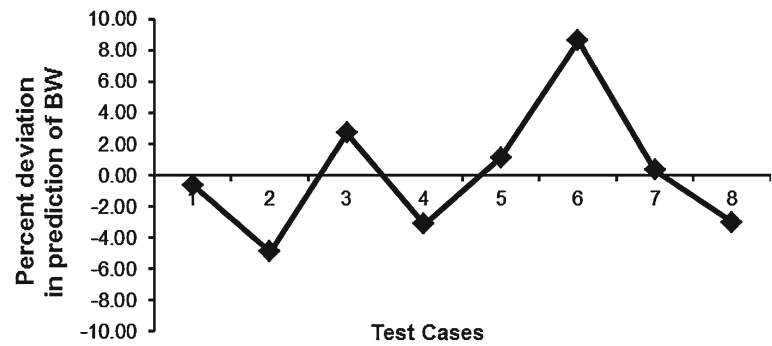**Fig. 10** Surface plots of BP with V, I and S

be done at high accelerating voltage and beam current, but at low welding speed to obtain the high depth of penetration.

The performance of the developed model was tested on eight test cases. Figure 11 displays the values of percent deviations in predictions of BP for the eight test cases. The maximum value of percent deviation in predictions of BP was found to be equal to 9.27 %. The average absolute percent deviation in predictions of BP was seen to be equal to 4.06.

Micro hardness (Hv) of the weld zone It was observed from the regression analysis for Hv that X_1, X_2, X_3, and X_1^2 were significant. The accelerating voltage was found to have non-linear relationship with Hv. Both the beam current and weld speed showed more or less linear relationships with Hv. The coefficient of correlation for the micro-hardness was obtained as 0.774. The adequacy of the model was also checked through the ANOVA test.

The un-coded form of Hv was found to be as follows:

$$
\begin{aligned}
HV_{un\text{-}coded} = {} & -3.94433 + 10.6468V - 6.93296I \\
& + 0.0501945S - 0.10165V^2 - 0.0156963I^2 \\
& - 3.67100E{-}05S^2 + 0.0150125VI \\
& - 5.72889E{-}04VS + 0.00451125IS \quad (7)
\end{aligned}
$$

Figure 12 shows the surface plots of micro-hardness (Hv) with accelerating voltage, beam current and welding speed. The Hv was seen to decrease with the beam current but increase with the weld speed. The increase in heat input decreases the cooling rate (Kannatey 2009), which in turn increases the grain size resulting in lower strength or micro-hardness values. The rate of cooling increases with the increase in welding speed (Kannatey 2009), which may be responsible for decrease in grain size and hence, increase in micro-hardness. The micro-hardness was found to initially increase with the accelerating voltage, but further increase in accelerating voltage resulted in a decrease of the micro-hardness. The increase in accelerating voltage increases the energy level of the electron and the centre-line temperature of the weld pool increases. This results in the increase in the cooling rate, which is proportional to the square of the temperature rise above the initial temperature (Kannatey

The surface plots of BP with accelerating voltage, beam current and welding speed are shown in Fig. 10. The bead penetration was found to increase with the increasing accelerating voltage and beam current. The BP could decrease with the high value of welding speed. Thus, the welding should

Fig. 11 Percent deviation in predictions of BP for the test cases
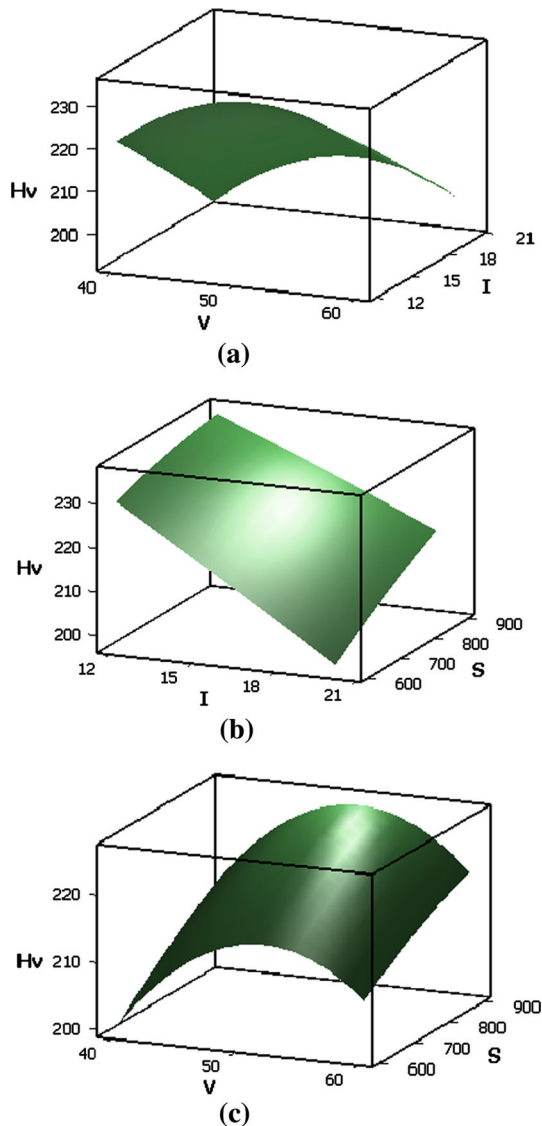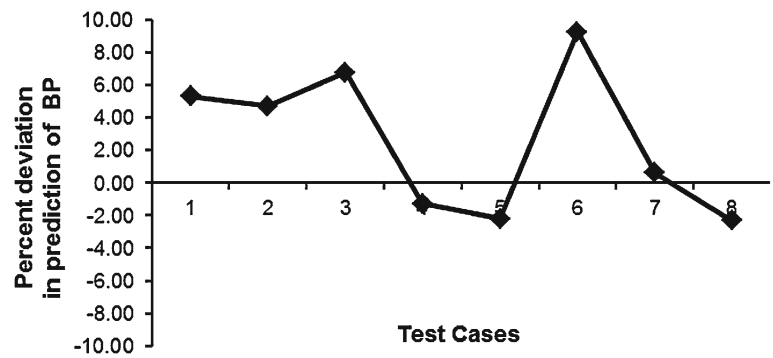

(a)

(b)

(c)

Fig. 12 Surface plots of Hv with V, I and S

2009). Therefore, the hardness values increase initially with an increase in the accelerating voltage. A further increase in the accelerating voltage results in the decrease of the focal spot diameter, which increases the incident power density. The increase in power density increases the heat input

and decreases the cooling rate. The decrease in cooling rate decreases the hardness value. Therefore, welding should be carried out at low beam current, medium accelerating voltage and high welding speed to obtain high micro-hardness and hence, high yield strength.

Figure 13 displays the values of percent deviations in predictions of Hv for the eight test cases. The maximum value of percent deviation in predictions of Hv was found to be equal to −9.69 %. The average absolute percent deviation in predictions of Hv had turned out to be equal to 6.79.

Results of Approach 2

A detailed parametric study was carried out to obtain optimal set of parameters for the developed BPNN model. Figure 14 shows the results of parametric study and the obtained optimized parameters for the BPNN model are displayed in Table 4.

The performance of the developed model was checked by passing the test cases through it. The values of percent deviation in prediction of the output parameters were recorded (refer to Fig. 15). Table 5 displays the average absolute percent deviation in predictions of different responses as obtained by this approach.

Results of Approach 3

The appropriate number of hidden neurons, and GA-parameters like population size, probability of mutation (p_m) and maximum number of generations (Gen_{max}), were obtained through a systematic parametric study, as shown in Fig. 16.

The optimal number of hidden neurons for the GANN model was obtained as 12, and the GA parameters, such as population size, maximum generations and probability of mutations were found to be equal to 200, 700 and 0.000095 respectively. The performance of the developed model was tested on eight test cases. The values of percent deviation in predictions of the responses are shown in Fig. 15. Table 5 shows the values of average absolute percent deviation in predictions of different responses as obtained by this approach.

Fig. 13 Percent deviation in predictions of Hv for the test cases
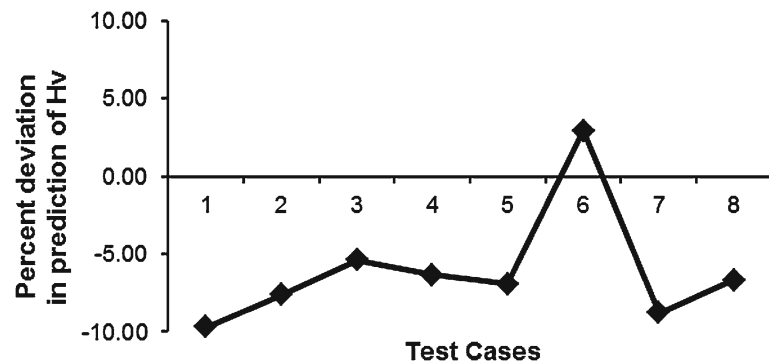
Results of Approach 4

The maximum number of runs for the PSONN-based model had been kept fixed to 50 after a few trial runs. The number of neurons in the hidden layer and that of executions or iterations in each run were kept equal to 30 and 15,000, respectively. The inertia weight w was determined as $w = 1/(\ln 2)$ and the cognitive and confidence coefficients were set as $c_1 = c_2 = (0.5 + \ln 2)$. Figure 17 shows the details of the parametric study carried out for the determination of number of hidden neurons and that of executions in each run.

The tested cases were passed through the developed PSONN model to check its performance. The values of percent deviation in prediction of different responses as obtained by this approach are displayed in Fig. 15. The average absolute percent deviations in prediction of different responses are displayed in Table 5.

Summary

All the developed four approaches could predict the responses reasonably well (within 10 %). However, the performance of BPNN was found to be slightly better than that of other NN-based approaches for two responses out of three. It might happen because their performances are generally found to be data-dependent. Moreover, the results of BPNN were seen to be comparable with those of regression analysis. Therefore, either the BPNN or regression analysis was recommended for the forward mapping of this process.

Results of reverse mapping

Reverse mapping of this welding process was also carried out using three NN-based approaches to predict the required process parameters in order to obtain a desired set of outputs or responses. Results of the reverse mapping are discussed below.

Results of Approach 1 (BPNN approach)

The optimal set of parameters for the BPNN model used for the reverse mapping are obtained through a systematic study, as shown in Table 6.

The test cases were passed through the optimized BPNN to check its performance for predicting the process parameters. The values of percent deviation in predictions of the process parameters are shown in Fig. 18.

Results of Approach 2 (GANN approach)

The parametric study of the GANN model was carried out to determine the set of optimal parameters corresponding to the best fitness. The optimal number of neurons in the hidden layer, population size, maximum number of generations and probability of mutation were found to be equal to 27, 50, 100 and 0.00095, respectively, for the developed network. The adequacy of the developed model was tested on eight test cases. The values of percent deviation in predictions of the process parameters are shown in Fig. 18.

Results of Approach 3 (PSONN approach)

The detailed parametric study was conducted to obtain optimum number of neurons in the hidden layer and number of executions or iterations in each run for the PSONN model. The optimum number of neurons of the hidden layer turned out to be equal to 28 and the optimum number of executions or iterations in each run was determined as 15,000. The performance of the tuned model was checked by passing through the test cases. Figure 18 shows the values of percent deviations in predictions of the process parameters corresponding to the set of desired outputs or responses.

Table 7 displays the values of average absolute percent deviation in predictions of different process parameters obtained using the BPNN, GANN and PSONN-based reverse models.
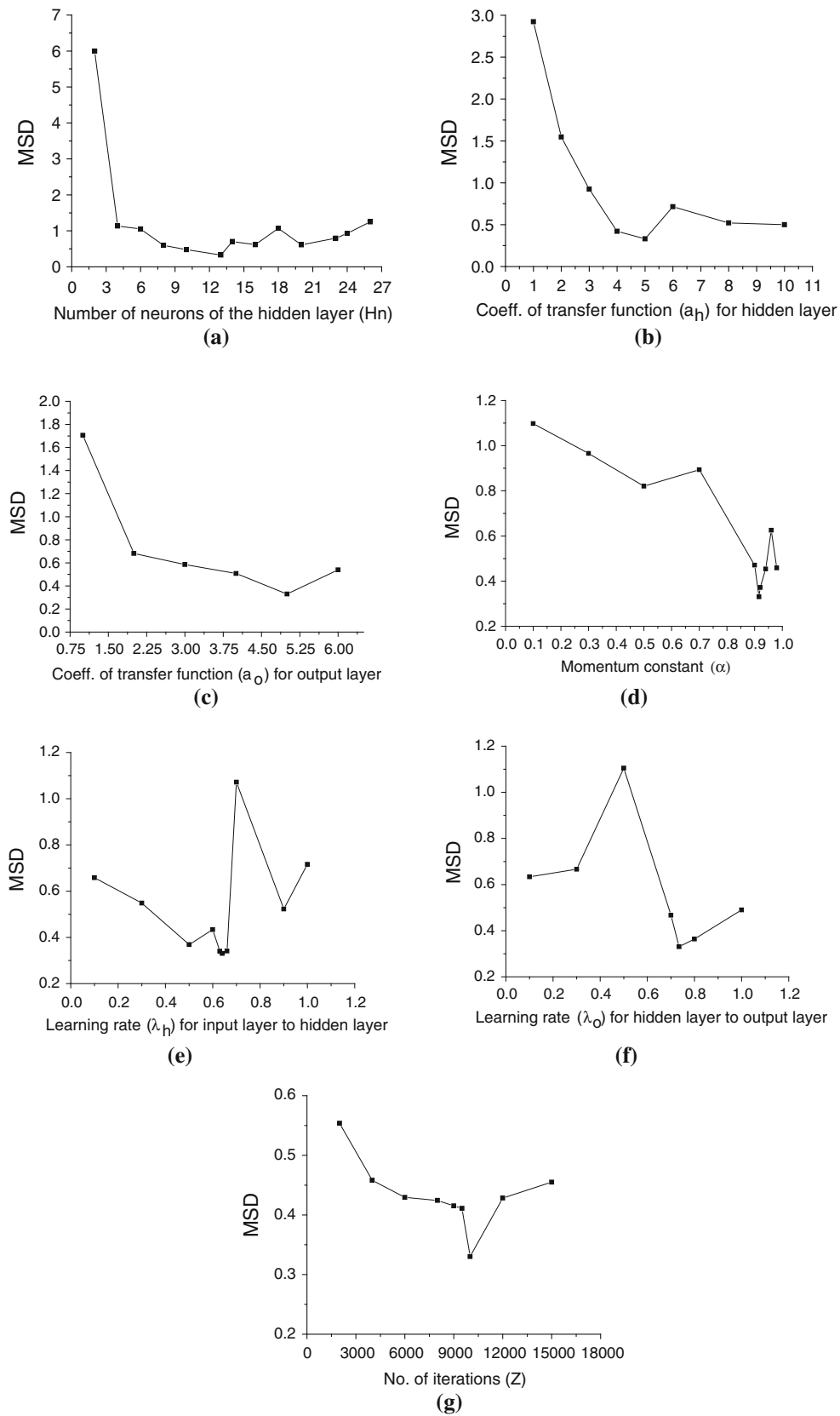
Fig. 14 Results of the parametric study conducted for the BPNN (**a–g**)

Table 4 Optimized parameters for BPNN-based forward model

Sr. no.	Parameters	Symbol	Value
1.	Number of neurons of the hidden layer	H_n	13
2.	Coefficients of transfer functions		
	For hidden layer	a_h	5.0
	For output layer	a_o	5.0
3.	Learning rate between		
	Input and hidden layers	λ_h	0.640
	Hidden and output layers	λ_o	0.735
4.	Momentum constant	α	0.916
5.	Bias	b	0.000009
6.	Maximum number of iterations	z	10,000

Fig. 15 Comparisons of different approaches in terms of percent deviation in predictions of various responses using regression analysis, BPNN, GANN and PSONN-based forward models (**a–c**)
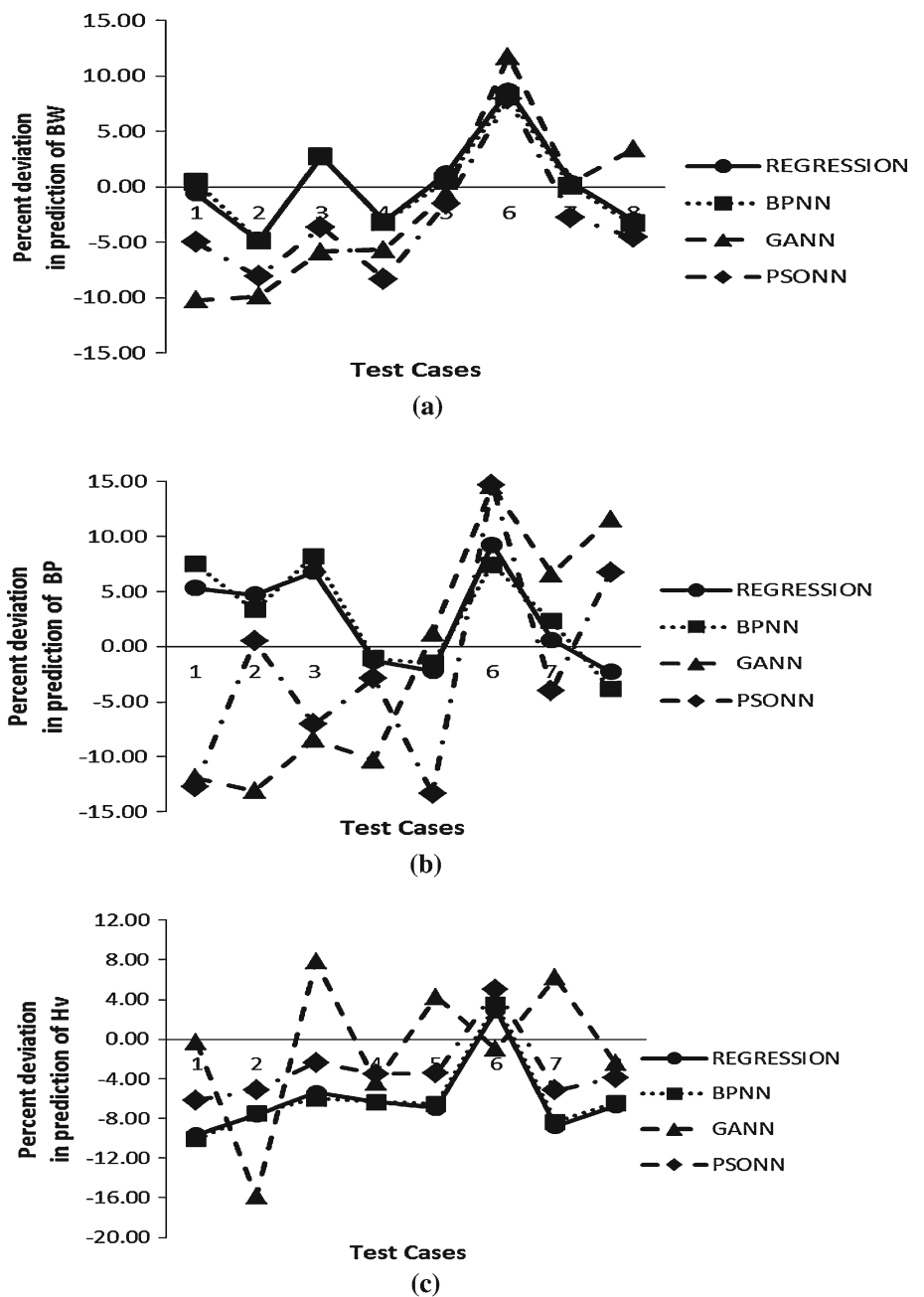
Springer

Table 5 Average absolute percent deviation in predictions of different responses using BPNN, GANN and PSONN-based forward models

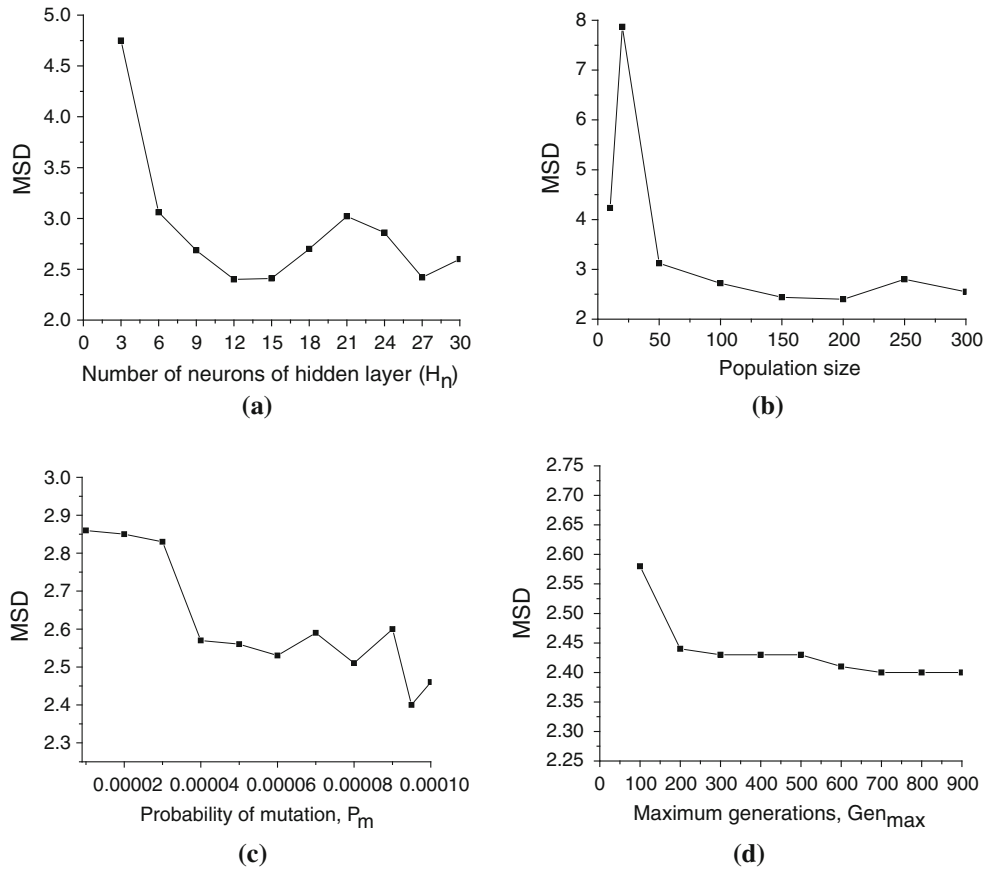| Sr. no.	Output or response	Average absolute % deviation using regression analysis	Average absolute % deviation using BPNN model	Average absolute % deviation using GANN model	Average absolute % deviation using PSONN model
1.	Bead Width, mm	3.07	2.91	5.98	5.23
2.	Bead Penetration, mm	4.06	4.39	9.70	7.74
3.	Vickers micro-hardness, VHN	6.79	6.85	5.29	4.34

Fig. 16 Results of the parametric study of the GANN approach (**a–d**)
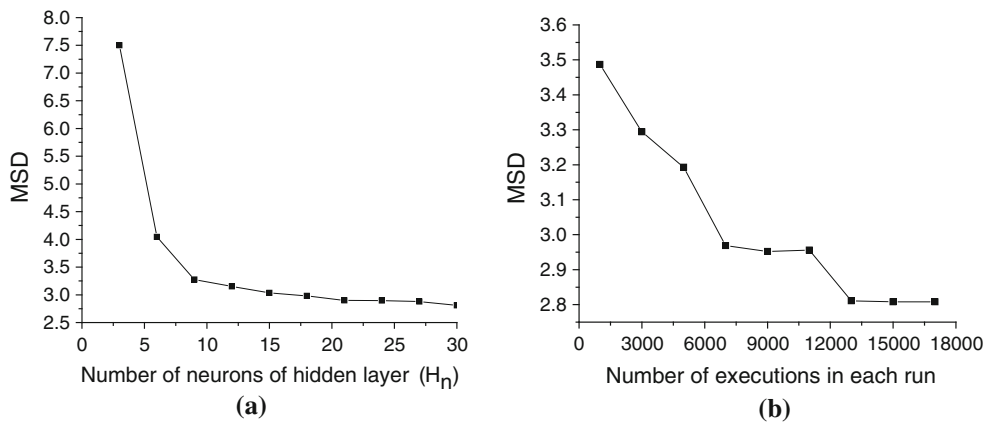

Fig. 17 Results of the parametric study of PSO-NN (**a**, **b**)

Table 6 Optimized parameters for BPNN-based reverse model

Sr. no.	Parameters	Symbol	Value
1.	Number of neurons of the hidden layer	Hn	10
2.	Coefficient of transfer function		
	For hidden layer,	a_h	6.5
	For output layer	a_o	2.5
3.	Learning rate between		
	Input and hidden layers,	λ_h	0.64
	Hidden and output layers	λ_o	0.20
4.	Momentum constant	α	0.25
5.	Bias	b	0.000009
6.	Maximum number of iterations	z	10,000

Fig. 18 Comparisons of different approaches in terms of percent deviation in predictions of various process parameters using BPNN, GANN and PSONN-based reverse models (**a–c**)
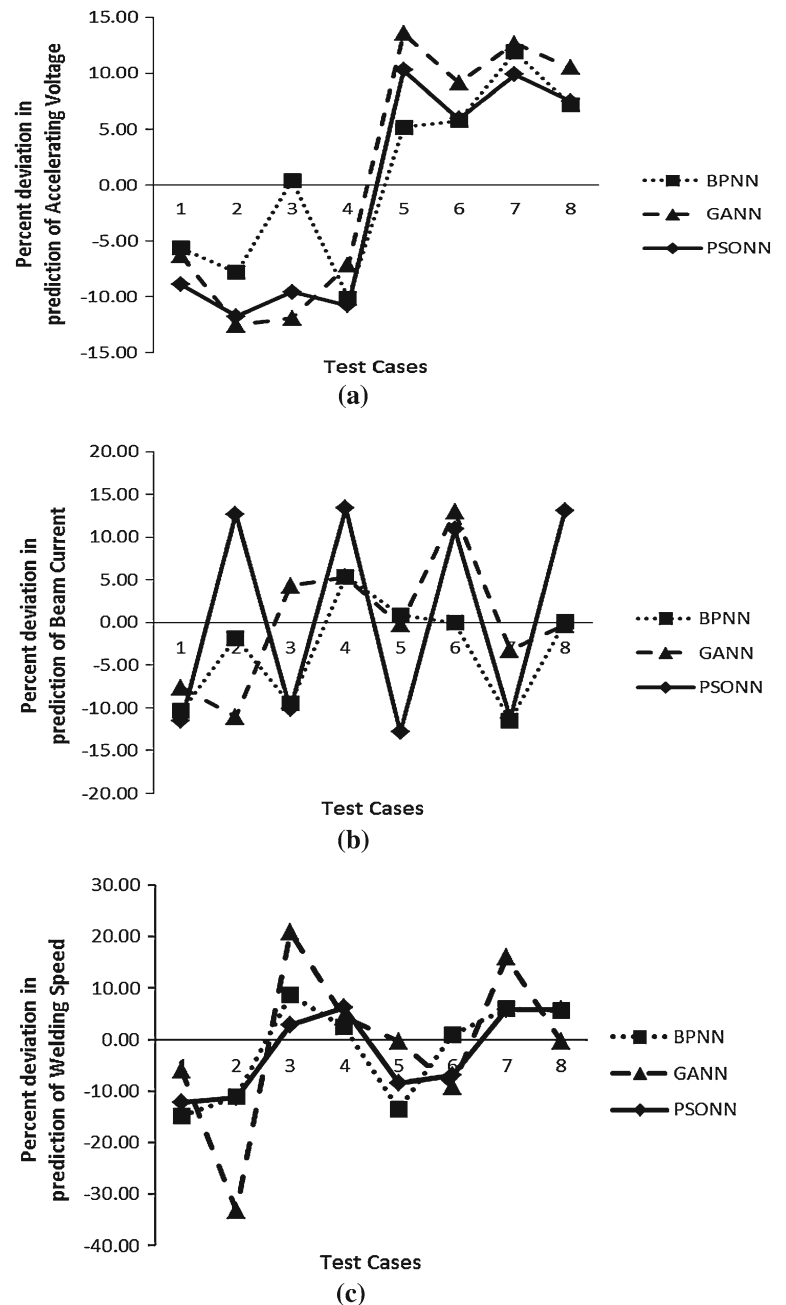
Table 7 Average absolute % deviation in predictions of different process parameters using BPNN, GANN and PSONN-based models for reverse mapping

Sr. no.	Process parameters	Average absolute % deviation using BPNN model	Average absolute % deviation using GANN model	Average absolute % deviation using PSONN model
1.	Accelerating voltage	6.75	10.46	9.32
2.	Beam current	4.94	5.64	11.97
3.	Weld speed	7.93	11.31	7.46

Summary

The performance of the BPNN and PSONN were found to be better than that of the GANN in most of the cases but not all. This indicates that the performances of these approaches are data-dependent. Although all the three NN-based approaches could tackle the problem of reverse mapping of this process, BPNN was recommended finally based on its performance in terms of accuracy in predictions.

Comparisons

Form the above study, it was observed that NN-based approaches could model the input-output relationships of this process accurately in both forward and reverse directions. The training of the NN-based approaches was done off-line and once the training was over, these approaches could yield the output(s) for a set of inputs within the fraction of a second in a P-IV PC. Thus, these approaches might be suitable for on-line implementations. Regression analysis carried out using Minitab-14 software, also did not take more than a second in the said PC. In order to capture the information of the process completely, all the outputs were to be modeled simultaneously, which could be done using the NN-based approaches. On the other hand, statistical regression analysis is conducted response-wise. It is important to mention that in order to automate any process, its input-output relationships are to be known accurately in both the forward and reverse directions on-line and NN-based approaches have the potential to serve this purpose. As the BPNN could perform better than other two NN-based approaches in case of both forward and reverse mappings, it was finally recommended for the input-output modeling of this process.

Concluding remarks

The electron beam welding of the reactive metal and its input-output modeling were carried out successfully in both forward and reverse directions. In this study, knowledge-based systems were developed using neural networks to establish the input-output relationships of this process. The following conclusions were drawn from this study.

- The forward models developed using regression analysis, BPNN, GANN and PSONN were found to be successful in predicting the responses in terms of bead width, bead penetration and micro-hardness of the fusion zone for a given set of process parameters.
- The reverse models developed using BPNN, GANN and PSONN were also seen to be efficient for the prediction of required process parameters, namely accelerating voltage, beam current and welding speed in order to obtain a desired set of outputs or responses.
- BPNN had been recommended for conducting both the forward and reverse mappings of this process.
- Knowledge-based systems developed using the neural networks could solve the problems of both forward and reverse mappings efficiently. The training of the neural networks-based approaches was done off-line and once the training was over, these approaches could yield the output(s) for a set of inputs within the fraction of a second in a P-IV PC. Thus, these approaches might be suitable for on-line implementations. Regression analysis carried out using Minitab-14 software, also did not take more than a second in the said PC. In order to capture the dynamics of the process completely, all the outputs are to be modeled simultaneously, which could be done using neural networks. On the other hand, statistical regression analysis was conducted response-wise. The developed neural networks-based approaches were able to make on-line predictions of the input-output relationships of the process accurately in both forward and reverse directions, which might be required for its automation.
- The welding should be carried out at low beam current and accelerating voltage and high welding speed to obtain low bead width.
- To ensure a high depth of penetration, welding is to be conducted at high accelerating voltage and beam current but at low welding speed.
- The high value of micro-hardness was obtained for the low beam current, medium accelerating voltage and high welding speed.

Scope for future work

Bead-on-plate welding experiment was carried out for the electron beam welding of Zircaloy-4 material. Actual butt welding will be tried for Zr-4 and other reactive metals, in future. The input-output modeling of the process may be carried out using other soft computing techniques.

Appendix: Photographs showing the shapes of fusion zone for some of the EB-welded samples of Zirclaoy-4
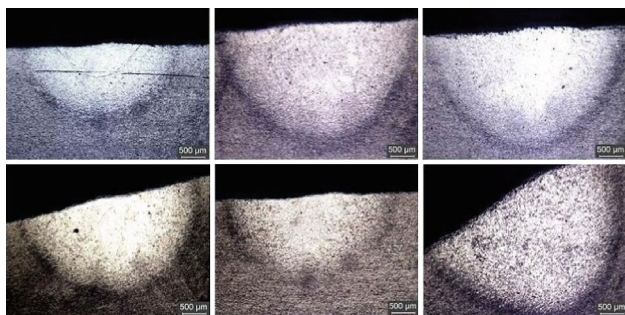
References

Ahmad, M., Akhter, J. I., Shaikh, M. A., Akhtar, M., Iqbal, M., & Chaudhary, M. A. (2002). Hardness and microstructural studies of electron beam welded joints of Zircaloy-4 and stainless steel. *Journal of Nuclear Materials*, *301*, 118–121.

Amarnath, M. V. V., & Pratihar, D. K. (2009). Forward and reverse mappings of TIG welding process using radial basis function neural networks (RBFNNs). In *Proceedings of IMechE, Part B: Journal of Engineering Manufacture* (Vol. 223, pp. 1575–1590).

Benyounis, K. Y., Olabi, A. G., & Hashmi, M. S. J. (2005). Effect of laser welding parameters on the heat input and weld-bead profile. *Journal of Materials Processing Technology*, *164–165*, 978–985.

Bhadeshia, H. K. D. H. (1999). Neural networks in materials science. *ISIJ International*, *39*(10), 967–975.

Chi, C. T., & Chao, C. G. (2007). Characterization on electron beam welds and parameters for AZ31B-F extrusive plates. *Journal of Material Processing Technology*, *182*, 369–373.

Choi, B. H., & Choi, B. K. (2008). The effect of welding conditions according to mechanical properties of pure titanium. *Journal of Materials Processing Technology*, *201*, 526–530.

Cook, G., Barnett, R. J., Andersen, K., & Strauss, A. M. (1995). Weld modeling and control using artificial neural networks. *IEEE Transactions on Industry Applications*, *31*(6), 1484–1491.

Dey, V., Pratihar, D. K., & Datta, G. L. (2010). Forward and reverse modeling of electron beam welding process using radial basis func-

tion neural networks. *International Journal of Knowledge-based and Intelligent Engineering Systems*, *14*(4), 201–215.

Dey, V., Pratihar, D. K., Datta, G. L., Jha, M. N., Saha, T. K., & Bapat, A. V. (2010). Optimization and prediction of weldment profile in bead-on-plate welding of Al-1100 plates using electron beam. *International Journal of Advanced Manufacturing Technology*, *48*, 513–528.

Dey, V., Pratihar, D. K., Datta, G. L., Jha, M. N., Saha, T. K., & Bapat, A. V. (2009). Optimization of bead geometry in electron beam welding using a Genetic Algorithm. *Journal of Materials Processing Technology*, *209*, 1151–1157.

Dutta, P., & Pratihar, D. K. (2007). Modeling of TIG welding process using conventional regression analysis and neural network-based approaches. *Journal of Materials Processing Technology*, *184*, 56–68.

Elmer, J. W., Giedt, W. H., & Eagar, T. W. (1990). The transition from shallow to deep penetration during electron beam welding. *Welding Journal*, *69*(5), 167s–176s.

Ganjigatti, J. P., Pratihar, D. K., & RoyChoudhury, A. (2007). Global versus cluster-wise regression analyses for prediction of bead geometry in MIG welding process. *Journal of Materials Processing Technology*, *189*, 352–366.

Gunaraj, V., & Murugan, N. (1999). Application of response surface methodology for predicting weld bead quality in submerged arc welding of pipes. *Journal of Materials Processing Technology*, *88*, 266–275.

Gunaraj, V., & Murugan, N. (1999). Prediction and comparison of the area of the heat affected zone for the bead-on-plate and bead-on-joint in submerged arc welding of pipes. *Journal of Materials Processing Technology*, *95*, 246–261.

Gunaraj, V., & Murugan, N. (2000). Prediction and optimization of weld bead volume for the submerged arc process—Part 1. *Welding Journal*, *78*, 286s–294s.

Gunaraj, V., & Murugan, N. (2000). Prediction and optimization of weld bead volume for the submerged arc process—Part 2. *Welding Journal*, *78*, 331s–338s.

Hashimoto, T., & Matsuda, F. (1965). Effect of welding variables and materials upon bead shape in electron beam welding. *Transactions of NIRM*, *7*(3), 96–109.

Ho, C. Y. (2005). Fusion zone during focused electron-beam welding. *Journal of Materials Processing Technology*, *167*, 265–272.

Huang, W., & Kovacevic, R. (2011). A neural network and multiple regression method for the characterization of the depth of weld penetration in laser welding based on acoustic signatures. *Journal of Intelligent Manufacturing*, *22*(2), 131–143.

Jha, M. N., Pratihar, D. K., Dey, V., Saha, T. K., & Bapat, A. V. (2011). Study on electron beam butt welding of austenitic stainless steel 304 plates and its input-output modeling using neural networks. In *Proceedings of IMechE, Part B: Journal of Engineering Manufacture* (Vol. 225, pp. 2051–2070).

Kannatey, E. A. (2009). Willey series on processing of engineering materials. In *Principles of laser materials processing*.

Kennedy, J., & Eberhart, R. (1995). Particle swarm optimization. In *Proceedings of IEEE International Conference on Neural Networks* (pp. 1942–1948). Perth, Australia.

Kim, D., Rhee, S., & Park, H. (2002). Modeling and optimization of a GMA welding process by genetic algorithm and response surface methodology. *International Journal of Production Research*, *40*(7), 1699–1711.

Kim, D., Kang, M., & Rhee, S. (2005). Determination of optimal welding conditions with a controlled random search procedure. *Welding Journal*, *90*(8), 125s–130s.

Klemens, P. G. (1969). Energy considerations in electron beam welding. *Journal of Electrochemical Society: Electochemical Science*, *116*(2), 196–198.

Koleva, E. (2001). Statistical modeling and computer programs for optimization of the electron beam welding of stainless steel. *Vacuum*, *62*, 151–157.

Koleva, E. (2005). Electron beam weld parameters and thermal efficiency improvement. *Vacuum*, *77*, 413–421.

Lancaster, J. F. (1970). *The metallurgy of welding, brazing and soldering*. London: George Allan and Unwin.

Lin, H. L. (2012). The use of the Taguchi method with grey relational analysis and a neural network to optimize a novel GMA welding process. *Journal of Intelligent Manufacturing*, *23*(5), 1671–1680.

Miyazaki, T., & Giedt, W. H. (1982). Heat transfer from an elliptical cylinder moving through an infinite plate applied to electron beam welding. *International Journal of Heat and Mass Transfer*, *25*(6), 807–814.

Mollah, A. A., & Pratihar, D. K. (2008). Modeling of TIG welding and abrasive flow machining processes using radial basis function networks. *International Journal of Advanced Manufacturing Technology*, *37*(9–10), 937–952.

Montgomery, D. C. (1997). *Design and analysis of experiments*. New York: Wiley.

Nagesh, D. S., & Datta, G. L. (2002). Prediction of weld bead geometry and penetration in shielded metal-arc welding using artificial neural networks. *Journal of Materials Processing Technology*, *123*, 303–312.

Okuyucu, H., Kurt, A., & Arcaklioglu, E. (2007). Artical neural network application to the friction stir welding of aluminum plates. *Materials and Design*, *28*, 78–84.

Olabi, A. G., Casalino, G., Benyounis, K. Y., & Hashmi, M. S. J. (2006). An ANN and Taguchi algorithms integrated approach to the optimization of CO2 laser welding. *Advances in Engineering Software*, *37*, 643–648.

Petrov, P., Georgiev, C., & Petrov, G. (1998). Experimental investigation of weld pool formation in electron beam welding. *Vacuum*, *51*, 339–343.

Pratihar, D. K. (2008). *Soft computing*. India, New Delhi: Narosa Publishing House.

Rao, K. P., Angamuthu, K., & Srinivasan, P. B. (2008). Fracture toughness of electron beam welded Ti6Al4V. *Journal of Materials Processing Technology*, *199*, 185–192.

Rudling, P., Strasser, A., & Garzarolli, F. (2007). Welding of Zirconium alloys, IZNA7 special topic report Welding of Zirconium Alloys.

Saha, T. K., & Ray. A. K. (2008). Vacuum—the ideal environment for welding of reactive materials. *Journal of Physics: Conference Series, 114*. doi:10.1088/1742-6596/114/1/012047.

Saresh, N., Pillai, M. G., & Mathew, J. (2007). Investigations into the effects of electron beam welding on thick Ti-6Al-4V titanium alloy. *Journal of Materials Processing Technology*, *192–193*, 83–88.

Tay, K. M., & Butler, C. (1997). Modelling and optimizing of a MIG welding process a case study using experimental designs and neural networks. *Quality and Reliability Engineering International*, *13*, 61–70.

Thomas, G., Ramchandra, V., Ganeshan, R., & Vasudevan, R. (1993). Effect of pre- and post-weld heat treatments on the mechanical properties of electron beam welded Ti-6Al-4V alloy. *Journal of Material Science*, *28*, 4892–4899.

Tonpe, S., Saibaba, N., Jayaraj, R. N., Ravi Shankar, A., Mudali, U. K., & Raj, B. (2011). Process development for fabrication of Zircaloy-4 dissolver assembly for reprocessing of spent nuclear fuel. *Energy Procedia*, *7*, 459–467.

Vijayan, T., & Rohatgi, V. K. (1984). Physical behaviour of electron-beam fusion heat transfer and deep penetration in metals. *International Journal of Heat and Mass Transfer*, *27*(11), 1985–1998.

Vitek, J. M., Iskander, Y. S., Oblow, E. M., et al. (1998). Neural network modeling of pulsed-laser weld pool shapes in aluminum alloy weld. In *Proceedings of 5th international conference on trends in welding research, Pine Mountain, GA* (pp. 442–448) June 1–5. ASM, International.

Yang, L. J., Bibby, M. J., & Chandel, R. S. (1993). Linear regression equations for modeling the submerged-arc welding process. *Journal of Materials Processing Technology*, *39*, 33–42.